Decomposition of Methanol on Clean and Oxygen-Predosed V(100): A First-Principles Study

ARTICLE *in* THE JOURNAL OF PHYSICAL CHEMISTRY C · NOVEMBER 2012

Impact Factor: 4.77 · DOI: 10.1021/jp307760a

5 AUTHORS, INCLUDING:

Hui Wang
Chinese Academy of Sciences
17 PUBLICATIONS **63** CITATIONS
SEE PROFILE

Chaozheng He
Nanyang Normal University
37 PUBLICATIONS **85** CITATIONS
SEE PROFILE

Jing-Yao Liu
Jilin University
148 PUBLICATIONS **736** CITATIONS
SEE PROFILE

THE JOURNAL OF PHYSICAL CHEMISTRY C

Article

pubs.acs.org/JPCC

Decomposition of Methanol on Clean and Oxygen-Predosed V(100): A First-Principles Study

Hui Wang,[†] Chao-zheng He,[†] Li-yuan Huai,[†] Fu-ming Tao,[‡] and Jing-yao Liu*[,†]

[†]Institute of Theoretical Chemistry, State Key Laboratory of Theoretical and Computational Chemistry, Jilin University, Changchun 130023, People's Republic of China

[‡]Department of Chemistry and Biochemistry, California State University, Fullerton, California 92834, United States

Supporting Information

ABSTRACT: The decomposition of CH_3OH on clean and oxygen-predosed V(100) surfaces was studied on the basis of periodic density functional calculations and microkinetic modeling. The results indicate that the O−H bond scission of CH_3OH is thermodynamically and kinetically favorable on clean V(100) while the C−H and C−O bond scissions are unlikely to occur at low temperature, and as a result, CH_3O is the major intermediate in the decomposition process. The C−O bond scission of CH_3O to form CH_3 is much easier than the C−H bond scission to form HCHO. Hydrogenation of CH_3 by the surface hydrogen from dissociating CH_3OH and CH_3O is responsible for the desorption of CH_4 at low and high temperatures, respectively. HCHO further undergoes decomposition or/and coupling to form CO or/and C_2H_4. When oxygen is preadsorbed on the surface at low coverage, the O−H bond scission of CH_3OH is virtually not affected, while the cleavages of the C−O and C−H bonds from CH_3O are inhibited in different degrees, leading to the decrease in the ratio of CH_4 produced at the low temperature relative to that at the high temperature. All products are delayed in temperature. The results are in good agreement with experimental observations.

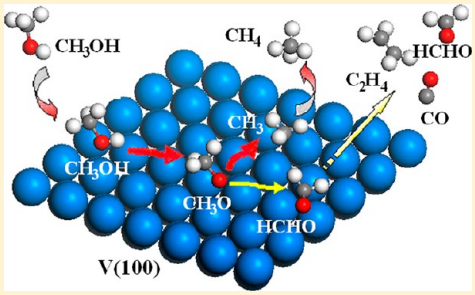

1. INTRODUCTION

The adsorption and decomposition of methanol (CH_3OH) on metal surfaces have attracted wide attention because of its potential applications such as in direct methanol fuel cells (DMFC)[1−7] and partial oxidation of methane (POM).[8] A large number of studies on reactions of CH_3OH with various pure metal surfaces[8−32] show that the activity of adsorbed CH_3OH is strongly dependent on the nature of metal surface. With late transition metals, the production of hydrogen and monoxide from methanol decomposition is generally favorable and is an efficient way to generate hydrogen in the context of fuel-cell technology as suggested. With early transition metals, on the other hand, the C−O bond scission is usually observed as a favorable dissociation step.

Vanadium oxides are important catalysts in some industrial processes such as POM[8,33,34] and are proposed to have suitable properties to catalyze the oxidative dehydrogenation of methanol. It is widely accepted that methoxy (CH_3O) is the key intermediate in these processes.[35−38] Recently, Shen and Zaera[38] studied the reaction of CH_3OH on clean and oxygen-predosed V(100) surfaces in ultrahigh vacuum (UHV) conditions by temperature-programmed desorption (TPD) and X-ray photoelectron spectroscopy (XPS). The O−H bond scission of CH_3OH to form CH_3O occurred first at about 260 K, followed by the C−O bond scission to yield methyl (CH_3) at 320 K or further dehydrogenation to form HCHO at 500 K. Methane (CH_4) was formed via hydrogenation of CH_3, and its desorption was observed in two regions of temperatures, around 320 and 490 K, respectively, and HCHO proceeded via desorption, self-coupling to form ethylene, or total dehydrogenation to form carbon monoxide. The experiment showed that the predosed oxygen below 0.3 ML modulated the reactivity of surface, resulting in an increased yield of high-temperature CH_4 at the expense of low-temperature CH_4 production and a delay of all surface reactions until a higher temperature was reached. All reaction yields were decreased when the oxygen coverage was beyond 0.3 ML because the development of vanadium oxide might reduce the number of available vanadium surface binding sites. The important effect of coadsorbed oxygen on the reaction of CH_3OH has also been found on other metal surfaces such as Ag,[31,39−41] Pd,[42] Au,[43] Cu,[23,44,45] and Ir[19] surfaces.

Although state-of-the-art experimental surface science techniques can provide some valuable information on the atomic level, a generally detailed description of the reaction has not been attained. Several theoretical studies have been reported on the chemisorption and decomposition of CH_3OH involving several metal surfaces such as Ge(100),[12] Ni(111),[20] Cu(100),[21,22] Cu(110),[22−24] Cu(111),[25,45] Pt(111),[26−28] Pd(111),[25,29] Rh(111),[30] Ag(111),[31] and Au(111).[32] However, no virtual theoretical study has been performed about the microscopic surface chemistry of CH_3OH

Received: August 6, 2012
Revised: October 26, 2012
Published: November 13, 2012

   dx.doi.org/10.1021/jp307760a | J. Phys. Chem. C 2012, 116, 25344−25353

on the V(100) surface. It is highly desirable to characterize the mechanistic details of the adsorption and decomposition processes of CH_3OH on V(100) in the search of better and more effective catalysts. In the present study, the reaction mechanisms of CH_3OH on V(100) surfaces are investigated using the periodic density functional theory (DFT) method. A range of issues will be analyzed, including the adsorption stability, site preference of CH_3OH, and the derived species on clean V(100). Transition states will be determined for all elementary reaction steps involved in the decomposition process. Details about the potential energy surface will be obtained for each step. Moreover, minimum energy paths will be identified for the dominant elementary steps on oxygen-predosed V(100). Finally, a microkinetic analysis will be made to estimate the likely decomposition mechanism and elucidate the role of coexisting oxygen on metal surface on the reaction pathways. The study aims for a fundamental understanding of the surface chemistry of methanol and methoxy groups adsorbed on vanadium surface.

2. COMPUTATIONAL DETAILS

Periodic DFT calculations with the Perdew–Burke–Ernzerhof (PBE)[46] generalized gradient approximation (GGA) were carried out with the Vienna ab initio simulation package (VASP),[47,48] and spin polarization was considered in all calculations. The one-electron wave function was expanded using a plane-wave basis set with an energy cutoff of 400 eV, and ion–electron interactions were described by the projector augmented wave (PAW)[49,50] method. Geometries were relaxed using the conjugate gradient algorithm until the forces on all unconstrained atoms less than 0.03 eV/Å. The force tolerance is adequate for our discussions based on some test cases, although if the convergence is further tightened to 0.01 eV/Å, the energy may change slightly (<0.02 eV), especially for the cases with small relative interaction energies. Brillouin zones were sampled with the (13 × 13 × 13) Monkhorst–Pack k-point for bulk calculation. The determined equilibrium lattice constant (a_0 = 2.9806 Å) is in good agreement with the experimental value (a_0 = 3.0240 Å).[51]

The V(100) surface was modeled by the slab supercell approach using (2 × 2) unit cells and a five-layer periodic slab separated by a vacuum region of 15 Å. Brillouin zones were sampled with the (6 × 6 × 1) Monkhorst–Pack k-point for surface calculations. The two upper V atom layers were allowed to fully relax at DFT-bulk geometry while the three lower layers were fixed.

The climbing-image nudge elastic band (CI-NEB) method[52,53] was used to locate transition states (TS), and the minimum energy pathways (MEPs) were constructed accordingly. The minima possess all real frequencies, and the transition states have only one imaginary frequency based on the vibrational analysis. Zero-point energy (ZPE) corrections were included in the barrier and reaction energy calculations. The adsorption energies (E_{ad}) for all possible adsorbates were calculated according to

$$E_{ad} = E_{gas-surf} - (E_{surf} + E_{gas})$$

where $E_{gas-surf}$, E_{surf}, and E_{gas} are the energies of the adsorbed species on V(100), the clean V(100) surface, and the corresponding gas-phase species, respectively. The interaction energy was defined as the difference between the energies of the coadsorbed configuration and infinite separation state (each adsorbate in separate unit cell at its most stable position). The reaction barriers and reaction energies of the elementary reaction steps were calculated with respect to the adsorbed reactants at the most stable sites with infinite separation, and the products at infinite separation were taken as the final state.

3. RESULTS AND DISCUSSION

Various configurations of CH_3OH and derived species were considered at three adsorption sites (top, bridge, and hollow) on V(100). Table 1 shows the most stable configurations and the corresponding adsorption sites and adsorption energies of the adsorbed species. All likely reaction paths were considered for each reaction, but only the minimum energy path is reported. In this section, we first present all elementary steps involved in the decomposition of CH_3OH and CH_3O on both clean and O-predosed V(100) surfaces and compared with those on other metal surfaces if the results are available. Figures 1–4 show the potential energy surfaces (PESs) along with the geometric configurations of the initial state (IS), transition state (TS), and final state (FS) in each step. To evaluate the effect of neighboring adsorbate molecules, we used a larger unit cell (3 × 3) corresponding to adsorbate surface coverage of 0.11 ML to examine the adsorption and dominant reaction steps and compared the results with those obtained by a (2 × 2) unit cell. We then present the possible formation pathways for the products CH_4, H_2, CO, C_2H_4, and H_2O from the decomposition fragments. Finally, a simple microkinetic model was developed on the basis of the computational results, which would ultimately identify the product selectivity and the effect of predosed O atom on surface.

Table 1. Geometric and Energetic Parameters of Reaction Intermediates as Identified Stable State

reaction intermediates	configurations	bond lengths (Å)	E_{ad}[a] (eV)
CH_3OH	top, O-bound	d(O–V) = 2.17	−0.60 (−0.57)
CH_2OH	bridge, C-bound and O-bound	d(C–V) = 2.03 d(O–V) = 2.28	−2.16 (−2.11)
CH_3O	bridge, O-bound	d(O–V) = 2.00	−3.88 (−3.71)[b]
HCHO	hollow, C-bound and O-bound	d(C–V) = 2.16 d(O–V) = 2.01	−2.57 (−2.52)[b]
CHO	hollow, C-bound	d(C–V) = 2.20	−4.59 (−4.51)[b]
CO	hollow, C-bound	d(C–V) = 2.20	−3.32 (−3.28)[b]
OH	bridge, O-bound	d(O–V) = 2.02	−4.77 (−4.66)
O	hollow	d(O–V) = 2.10	−8.43 (−8.36)
H	hollow	d(H–V) = 2.21	−2.91 (−2.80)
CH_3	bridge C-bound	d(C–V) = 2.23	−2.17 (−2.07)[b]
CH_4	bridge, H-bound	d(H–V) = 3.33	−0.04 (0)[b]
C_2H_4	hollow, C-bound	d(C–V) = 2.21	−1.18 (−0.57)[b]
H_2O	top O-bound	d(O–V) = 2.20	−0.65 (−0.60)
H_2	top	d(H–V) = 2.00	−0.18 (−0.11)

[a]Values in parentheses include ZPE correction. [b]Values are taken from our previous work, ref 58.

3.1. Decomposition Pathways on Clean V(100).

3.1.1. Adsorption and Decomposition of CH_3OH. The CH_3OH molecule was found stable only at the top site with an adsorption energy of −0.57 eV. As shown in Figure 1, it binds to the surface through the O atom. The C–O bond is inclined in an angle of 34° from the surface normal and the O–H bond is oriented toward a hollow site. The geometry parameters of adsorbed methanol remained essentially constant from 0.11 to 0.25 ML, and the adsorption energy without ZPE

dx.doi.org/10.1021/jp307760a | J. Phys. Chem. C 2012, 116, 25344–25353

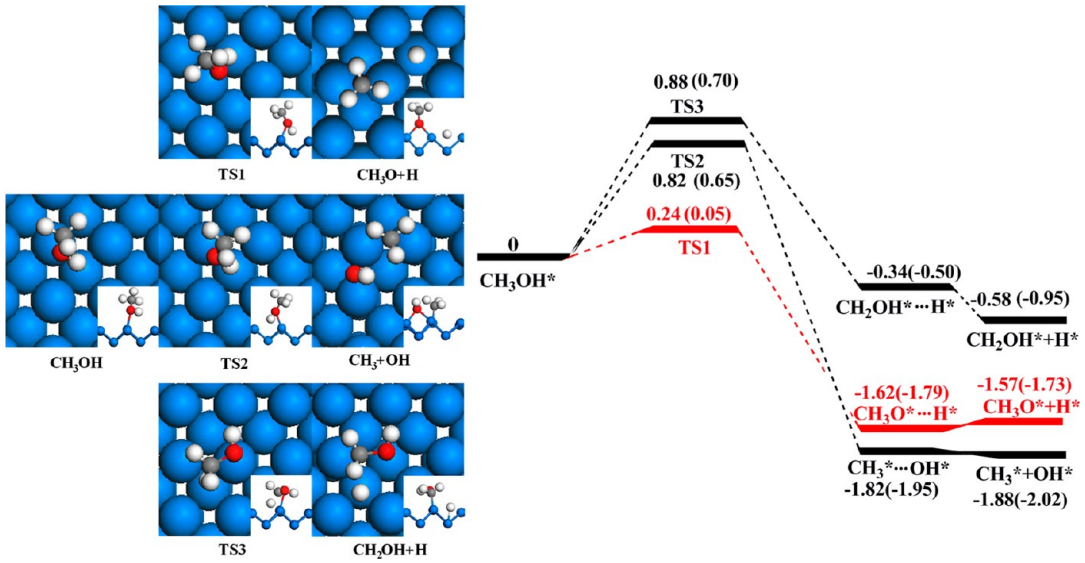

Figure 1. Decomposition pathways of CH_3OH on clean V(100). Values in parentheses include ZPE correction.

is slightly larger at 0.11 ML (−0.71 eV vs −0.60 eV). The two bonds are elongated by 0.02 and 0.03 Å, respectively, from those in the gas phase while the C−H bond length remains nearly the same. The adsorption configuration is similar to that on other surfaces. The adsorption energy on V(100) is similar to those on Rh(111) (−0.64 eV)[30] and Au(111) (−0.59 eV),[32] while it is much larger than those on Cu(110) (−0.41 eV),[22] Pd(111) (−0.39 eV),[25] Pt(111) (−0.33 eV),[27] Cu(100) (−0.21 eV),[22] Cu(111) (−0.17 eV),[25] Ni(111) (−0.16 eV),[20] Ag(111) (−0.15 eV),[31] and Ge(100) (−0.11 eV).[12] Three decomposition pathways of the adsorbed CH_3OH molecule were considered involving the scissions of the O−H, C−O, and C−H bonds.

The O−H scission pathway is characterized by its transition state TS1, as shown in Figure 1. The dissociating O−H bond is stretched from 1.00 to1.25 Å at the transition state. Beyond the transition state, the H atom of the dissociating bond moves to its favorable hollow site, while the O atom of the nascent CH_3O fragment approaches to a neighboring V atom to form a bridge configuration. This step is both kinetically and thermodynamically very feasible because of the small barrier (0.05 eV) and large exothermicity (−1.73 eV). The barriers without ZPE obtained at the coverages of 0.11 and 0.25 ML are very similar (0.26 eV vs 0.24 eV).

The C−O bond inclines to the surface and then dissociates to form CH_3 and OH via a transition state, TS2, which is characterized by a C−O bond length of 2.00 Å, elongated by about 38% from that of the initial reactant. Beyond the transition state, the CH_3 group binds at the bridge site via the C atom and OH moves to the adjacent bridge site. The site preference for each product remains invariant with respect to adsorption in separate unit cells. The calculated energy barrier for this reaction step is 0.65 eV, and the calculated reaction energy is −2.02 eV.

The C−H bond closer to the surface is activated due to the incline of the C−O bond. It breaks to form hydroxymethyl (CH_2OH) and atomic hydrogen via a transition state, TS3. The dissociating C−H bond is elongated to 1.45 Å at TS3 from 1.10 Å at the initial reactant. Beyond the transition state, the C atom binds to another V atom, forming an $\eta^1(C)-\eta^1(O)$ configuration of CH_2OH with the C and O atoms adsorbed parallel to two adjacent V atoms on the surface. Such a configuration is the only stable one for CH_2OH on the surface with an adsorption energy of −2.11 eV. The H atom dissociated from the process moves to a hollow site. The process has a barrier of 0.70 eV and is exothermic by 0.95 eV.

It is seen from the PES in Figure 1 that the O−H bond scission is the most favored pathway in kinetics because of the smallest energy barrier (0.05 eV) and the intermediate CH_3O from O−H bond scission is more stable than its isomer CH_2OH from C−H bond scission, thus more thermodynamically favorable. On the other hand, although the formation route of methyl or CH_2OH (with the corresponding energy barriers of 0.65 or 0.70 eV) is indeed active at high temperature (above 300 K), the rate ratio between the O−H and C−O (or C−H) bond scission paths, which can be described by the relation $r_1/r_2 = k_1\theta_{CH_3OH}\theta_*/k_2\theta_{CH_3OH}\theta_* = k_1/k_2 \approx \exp[(E_{a2} - E_{a1})/RT]$, shows that the former one is dominant at the temperature below 1000 K. Also it is noted that, due to the relatively weak interaction of methanol on V(100) (with the adsorption energy E_{ad} = −0.57 eV), the desorption of the methanol would be favored over the C−O or C−H bond scission. So the O−H bond scission to produce CH_3O is a major path for the decomposition of CH_3OH on clean V(100), and the other two bond scissions are unlikely to occur at low temperature. For this reason, only the reaction pathways originating from the intermediate CH_3O were pursued in the present study. With a simple rule-of-thumb method (around 200 K for a barrier of 0.50 eV and 300 K for a barrier of 0.75 eV),[54] it can be estimated that the O−H bond scission of methanol occurs below 100 K for a barrier of 0.05 eV. The estimate is in quite reasonable agreement with the experiment in which the CH_3O radical was detected as the major intermediate from the dehydrogenation of CH_3OH at a low temperature, <260 K.[38]

It is found that the order of reactivity of the three bonds on Ge(100)[12] is the same as that on V(100) because of similar atomic number. In comparison with the activation of methanol on Cu surfaces, Cu(100),[22] Cu(110),[22] Cu(111),[25] and on Ni(111),[20] O−H activation is also the most favorable with small energy barriers of 0.34, 0.73, 0.17, and 0.40 eV, respectively. Similar cases can be found from experiments on

dx.doi.org/10.1021/jp307760a | J. Phys. Chem. C 2012, 116, 25344−25353

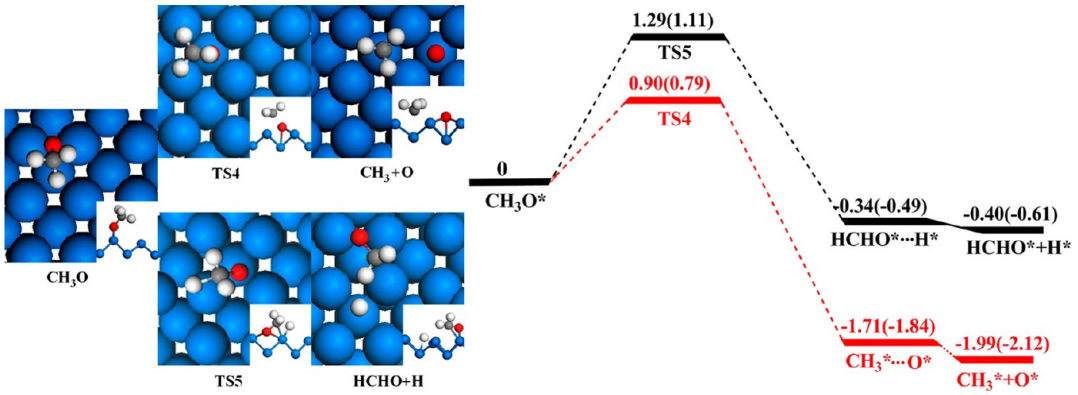

Figure 2. Decomposition pathways of CH_3O on clean V(100). Values in parentheses include ZPE correction.

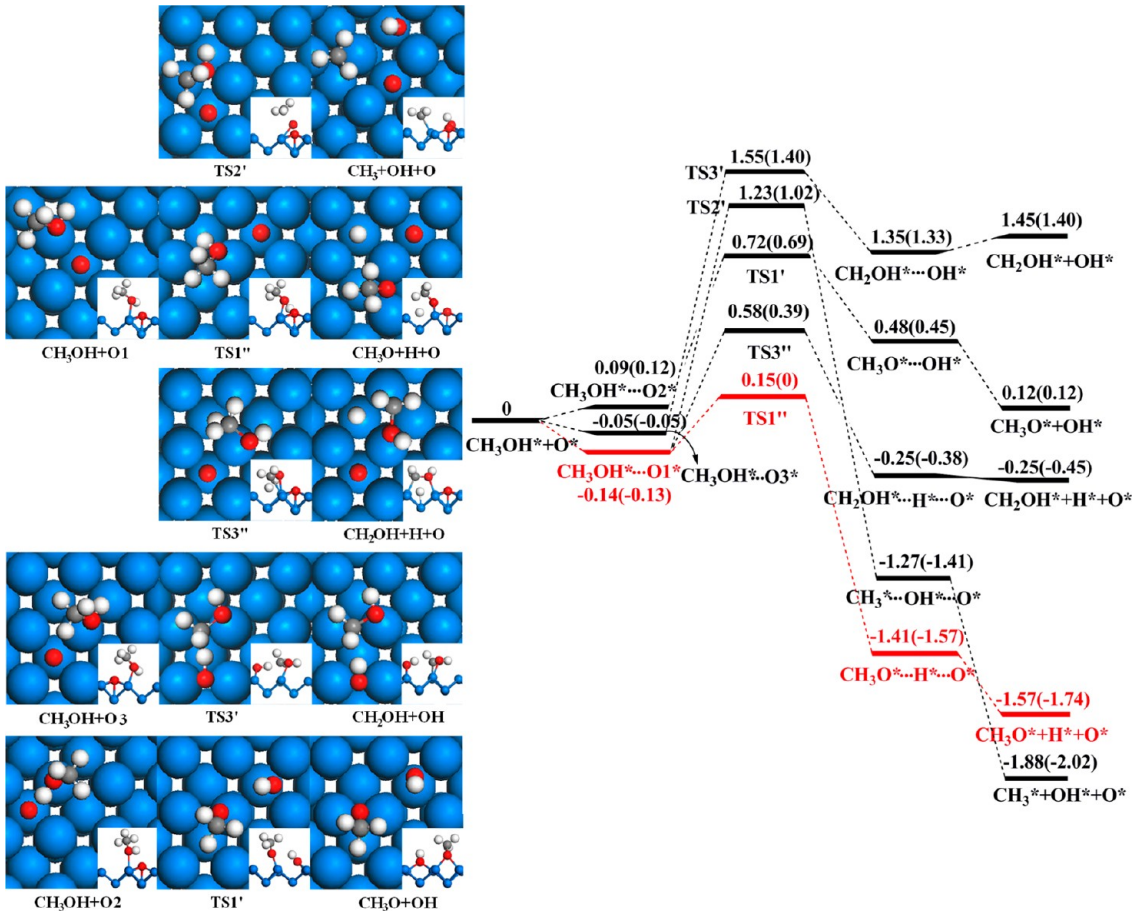

Figure 3. Decomposition pathways of CH_3OH on O-predosed V(100). Values in parentheses include ZPE correction.

Au(310)[17] and Ru(001),[15] as well as on Au(111)[32] and Ag(111),[31] although the O−H bond scission is indeed inhibited due to large energy barriers, 1.27 and 1.67 eV, respectively, on the latter two surfaces. However, the case is different on Pt(111)[26−28] and Pd(111):[29] C−H activation with smaller energy barrier becomes favored over the O−H activation. On Rh(111),[30] both O−H and C−H bond scissions are favorable with comparable energy barriers (0.95 and 0.93 eV). Among all these studied metal surfaces, the C−O bond scission of methanol is the least favorable, which has been considered by few theoretical studies.

3.1.2. CH_3O Decomposition. The CH_3O radical prefers to adsorb at the bridge site through the O atom with an adsorption energy of −3.71 eV. The value decreases slightly from the coverage of 0.25 to 0.11 ML (−3.88 eV vs −3.92 eV, without ZPE). The adsorption stability on metal surfaces follows the order of V(100) > Cu(110) > Rh(111) ≅ Cu(111) > Ag(111) ≅ Pd(111) ≅ Pt(111) > Au(111) with the values 3.88, 2.98,[22] 2.48,[30] 2.45,[25] 1.85,[31] 1.73,[25] 1.54,[26] and 1.02 eV,[32] respectively. CH_3O can undergo the C−O bond scission via the transition state TS4 to produce a CH_3 radical with an energy barrier of 0.79 eV and a strong exothermicity of 2.12 eV. The details have been described in our previous work.[58] The barrier without ZPE becomes smaller at the coverage of 0.11 ML (0.82 eV) than that at the coverage of 0.25 ML (0.90 eV).

dx.doi.org/10.1021/jp307760a | J. Phys. Chem. C 2012, 116, 25344−25353

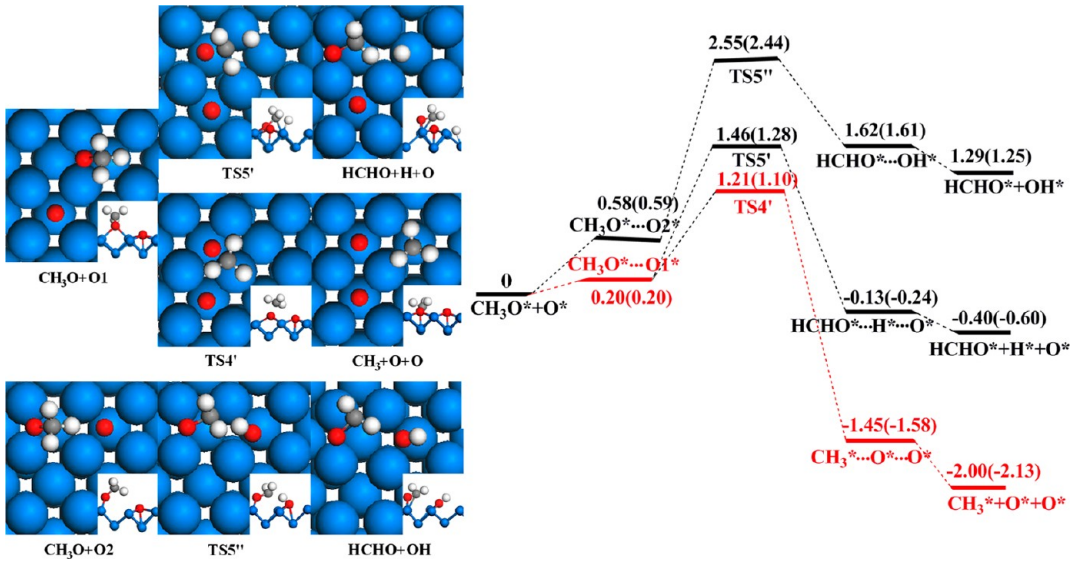

Figure 4. Decomposition pathways of CH_3O on O-predosed V(100). Values in parentheses include ZPE correction.

The CH_3O radical can also undergo the C−H bond scission to produce HCHO via the transition state TS5 in which the C−H bond is elongated by 36% from that of the initial state. Beyond the transition state, the dissociating H atom diffuses to a hollow site and the O atom of the nascent HCHO approaches to a bridging site to form a stable configuration with the C−O bond nearly parallel to the surface, similar to the case in separate unit cell. This step is modestly exothermic by 0.61 eV, and the energy barrier is 1.11 eV, which compared well with the value of 1.14 eV at the coverage of 0.11 ML.

It is clear that the C−O bond scission of CH_3O to produce CH_3 is thermodynamically and kinetically more favorable than the C−H bond scission leading to HCHO for the smaller barrier, 0.79 eV, compared to 1.11 eV, and larger exothermicity, 2.12 eV, compared to 0.61 eV. Applying the simple rule-of-thumb method mentioned above, the C−O bond scission of CH_3O occurs around 316 K and the C−H bond scission occurs around 444 K. This result strongly supports the experimental speculation that the C−O bond scission occurs at 320 K while the C−H bond scission occurs around 500 K.[38] Different from the case on V(100), the C−O bond scission of CH_3O is found unlikely on the majority of metal surfaces studied experimentally and theoretically, such as Cu,[24] Rh,[30] Pt,[27] Pd,[9] Ni,[18,20] Ag,[11,31] and Au,[13,32] while the C−H bond scission is more favorable on these metal surfaces.

3.2. Effect of Predosed Oxygen on Decomposition Pathways. The oxygen atom produced from the C−O bond scission of CH_3O may be deposited on the surface during the reaction because of the high desorption energy, 8.36 eV. The reduction of the oxygen to OH is also not feasible because of a large barrier of 2.27 eV. The accumulation of the resulting oxygen on the surface likely alters the selectivity of products, which was confirmed by experiment.[38] The effect of coadsorbed O atoms on the decomposition of CH_3OH and CH_3O is discussed as follows.

3.2.1. Decomposition of CH_3OH on Oxygen-Predosed V(100). The coadsorbed O atom may participate in the dehydrogenation of CH_3OH via the H-abstraction reaction. For the O−H bond scission, the H-abstraction reaction starts from the coadsorption of CH_3OH and O (see Figure 3) with a repulsion energy of 0.12 eV. In the following step, the O atom abstracts the hydroxyl hydrogen via a late transition state TS1′, at which the breaking O−H bond is 2.68 Å and the nascent H−O bond length is 0.98 Å. Finally, the nascent CH_3O and OH move away, both situated at bridge sites. The complete reaction has an energy barrier of 0.69 eV and is endothermic by 0.12 eV relative to the reactants at infinite separation. For the C−H bond scission of CH_3OH, the H-abstraction reaction starts from the coadsorbed state of CH_3OH and O (see Figure 3) with an attraction of 0.05 eV and passes through the transition state TS3′ to the final state, in which CH_2OH locates at the bridge site in the disigma mode and OH moves to the adjacent bridge site. This step has to overcome a barrier as high as 1.45 eV relative to the coadsorption initial state.

Alternatively, the coadsorbed O atom does not react with CH_3OH, only serving as a spectrator on the surface. As shown in Figure 3, the initial state for the bond scissions of CH_3OH was chosen to be the most stable coadsorption configuration with the O atom at the farther hollow site. There is a small attraction between the O atom and CH_3OH, −0.13 eV with ZPE correction and −0.14 eV without ZPE, while the interaction is repulsive at the coverage of 0.11 ML, 0.11 eV without ZPE. The O−H bond breaks via the transition state TS1″, and the final state FS is similar to that on the clean V(100) surface except for the O atom at the initial hollow site. This dehydrogenation reaction is a very facile step, with essentially a barrier of 0.13 eV and being exothermic by 1.61 eV relative to the coadsorption initial state. The barrier is calculated to be 0.16 eV (without ZPE) at the coverage of 0.11 ML relative to the state of infinite separation. Similar processions can be found for the C−O and C−H bond scission of CH_3OH. The energy barriers are 1.15 and 0.52 eV, respectively, and the reactions are exothermic by 1.89 and 0.32 eV, respectively.

These calculated results show that the direct dehydrogenation of CH_3OH is more favorable than the H-abstraction reaction in kinetics and thermodynamics at the O coverage of 0.25 ML. Also, the direct C−H bond scission of CH_3OH is slightly enhanced for the smaller barrier (0.52 eV vs 0.70 eV), and the C−O bond scission is inhibited (1.15 eV vs 0.65 eV), while the O−H bond scission is virtually not affected (0.13 eV vs 0.05 eV) by the coexistence of surface oxygen, and same as

dx.doi.org/10.1021/jp307760a | J. Phys. Chem. C 2012, 116, 25344−25353

on the clean surface. This dissociation step is the most favorable one in CH_3OH dissociation process, and as a result, CH_3O is still the key intermediate on the O-predosed surface. Different from the surface oxygen involved in the decomposition of CH_3OH on V(100), on Cu(111),[45] Cu(110),[23] and Ag(111),[31] the presence of oxygen strongly promotes the O−H bond scission of methanol by the oxygen-assisted dehydrogenation.

3.2.2. CH_3O Decomposition on Oxygen-Predosed V(100). Two reaction paths were located for the C−H bond scission of CH_3O, similar to the dehydrogenation of CH_3OH on O-predosed surface. The H-abstraction reaction starts from the coadsorption of CH_3O and O (see Figure 4) with a strong repulsion energy of 0.59 eV. The O atom then abstracts the H atom closer to the surface to produce HCHO and OH at their favorite sites by overcoming a high energy barrier of 2.44 eV, and the reaction is endothermic by 1.25 eV. The second path is initiated from the most stable coadsorption state (see Figure 4), which is about 0.20 eV less stable than the infinite separation state. The value at the coverage of 0.11 ML is smaller (0.14 eV vs 0.20 eV without ZPE). The direct C−H bond scission overcomes a barrier of 1.28 eV via TS5′ with the reaction energy of −0.60 eV, while the C−O dissociation of CH_3O occurs via TS4′ with a barrier of 1.10 eV and an exothermicity of −2.13 eV. The barriers without ZPE are 1.08 and 1.27 eV for the two steps at the coverage of 0.11 ML, respectively, and are slightly lower than those (1.21 and 1.46 eV) at the coverage of 0.25 ML. Similar to the case of CH_3OH, the direct C−H bond scission of CH_3O is preferred for a smaller barrier over the H-abstraction reaction by the surface O atom. Contrasted with cases on the clean surface, the C−H and C−O bond scission processes are both slightly inhibited because of the increased energy barriers of 0.17 and 0.31 eV, respectively. As a result, the decomposition of CH_3O may be delayed to a higher temperature in the presence of O atoms on the surface. In contrast, on Cu(111),[45] Cu(110),[23] and Ag(111),[31] the presence of adsorbed oxygen strongly enhances the C−H bond scission of CH_3O by lowering the reaction barrier via the oxygen-assisted dehydrogenation.

3.3. Analysis of the Effect of Predosed Oxygen on Methanol Decomposition. The results so far indicate that adsorbed methanol may proceed via one of the following routes: $CH_3OH \rightarrow CH_3O \rightarrow CH_3$ and $CH_3OH \rightarrow CH_3O \rightarrow$ HCHO. The former route is preferred over the latter on clean and O-predosed surfaces. The dehydrogenation of CH_3OH to CH_3O is very facile while the following dissociation of CH_3O is a difficult step. The coexistence of surface oxygen may increase the barriers for the C−O and C−H bond scission steps of CH_3O by 39% and 15%, respectively, from those on clean surface. It suggests that the C−O and C−H bond scissions of CH_3O are inhibited in different degrees, leading to the change of ratio between the product yields at different temperatures. It is found that the deviation is small in the calculated results between the coverages of 0.25 and 0.11 ML, and thus the conclusions at the two coverages are the same. Moreover, the surface O atoms may inhibit the dissociation steps because of site blocking. These two factors may result in a delay in the decomposition of CH_3O to higher temperature in the presence of O atoms on the surface, which is consistent with experimental observations.[38]

The H-abstraction reactions of CH_3OH or CH_3O by surface O atoms are less favorable than the direct bond scissions, suggesting that the surface O atoms may not be directly involved in the decomposition process and it may only affect the reactions via site-blocking or redistribution of electronic density within the adsorbed species. To testify the redistribution of electronic density between the adsorbed species and the surface, Bader analysis on the adsorption systems was performed with Bader's program.[55−57] Figure 5 shows plots of

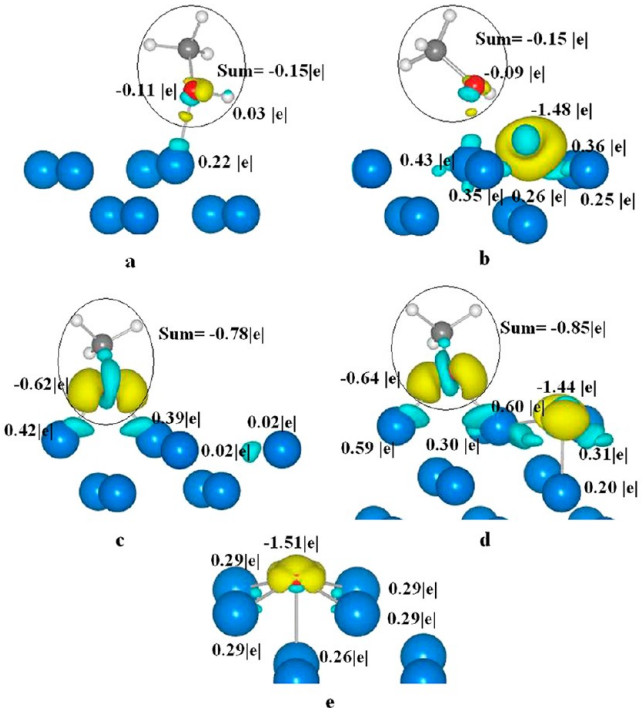

Figure 5. Charge-density difference for CH_3OH and CH_3O on clean and O-predosed V(100). Isosurfaces are calculated at 0.01 e Å^3. (a) CH_3OH adsorbed on clean V(100). (b) CH_3OH adsorbed on O-predosed V(100). (c) CH_3O adsorbed on clean V(100). (d) CH_3O adsorbed on O-predosed V(100). (e) O adsorbed on V(100).

the contour surface of the electron-density difference, Δ_{diff} = [gas−surface] − ρ[surface]− [gas] for CH_3OH and CH_3O. The Bader charge analysis for the adsorption of species on clean V(100) shows that, upon adsorption, the species become negatively charged whereas the surface becomes positively charged. When an oxygen atom is adsorbed on the surface, the electronic charges are redistributed. More electronic charge is transferred from the surface to the predosed oxygen. On the other hand, the change of electronic charge of the adsorption species is very small. The vanadium atoms at the topmost layer of V(100) behave as an acceptor center of electrons from the oxygen atom of methanol/methoxy and become more positively charged due to the electron transfer from the surface to the preadsorbed oxygen atom. As a result, the charge−charge interaction becomes stronger between the adsorption species and the surface. The enhanced charge−charge interaction has a positive effect on the increase in the binding energy.

3.4. Formation of Products. *CH_4 and H_2.* The key intermediate CH_3, which is produced by the decomposition of CH_3OH, can undergo hydrogenation to yield CH_4, which desorbs from the surface easily because of its zero adsorption energy. As described in our previous work, this step needs to overcome a barrier of 1.03 eV (0.88 eV relative to the coadsorbed IS) and is endothermic by 0.54 eV.[58]

Molecular hydrogen (H_2) can form by the coupling of H atoms on the surface. Two H atoms at adjacent hollow sites

dx.doi.org/10.1021/jp307760a | J. Phys. Chem. C 2012, 116, 25344−25353

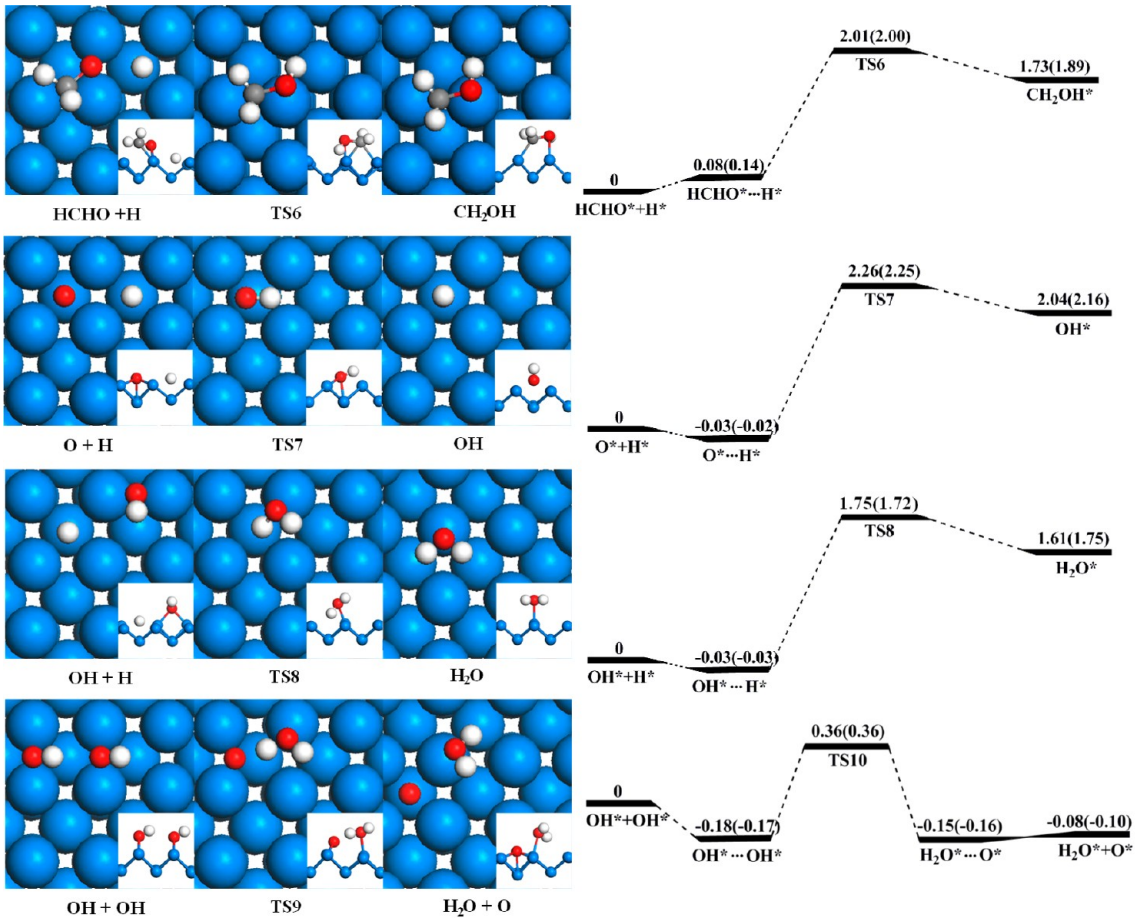

Figure 6. Reaction pathways for the formation of CH_2OH and H_2O on V(100). Values in parentheses include ZPE correction.

need to overcome a barrier of 1.37 eV to yield H_2 at the bridge site, which is a physical adsorption state with a small adsorption energy of −0.02 eV. Since the potential energy surface shows a rather flat region around the energy maximum, the exact identification of the transition state structure was not feasible.

The CH_4 and H_2 formation paths are both endothermic, and the entropic contributions to the Gibbs free energies at the transition state plays an important role at UHV condition (10^{-13} atm) in the experiment.[38] The transition state for the desorption coupling of adsorbed H atoms is very close to the gas phase H_2, so entropic effect is the main driving force for the process. As discussed above, CH_3 may form from the C−O bond scission of CH_3O at 316 K, and the H atom may form from the O−H bond scission of CH_3OH below 100 K or from the dehydrogenation of CH_3O around 444 K. One might anticipate that, at the temperature lower than 316 K, only H atoms are formed on the surface and then combined to form H_2. As the temperature increases (above 316 K), CH_3 forms and the surface H atom prefers to react with CH_3 to yield CH_4 because of a rather small barrier, instead of forming H_2. The lack of surface hydrogen may cause CH_3 to remain on the surface until H atoms are released from the dehydrogenation of CH_3O at high temperatures. Two regions of CH_4 desorption were observed from experiments as a result of the lack of H atoms on the surface in the intermediate temperatures.[38] When oxygen is predosed on the surface, the C−H and C−O bond scissions of CH_3O are delayed to higher temperatures, and the ratio of the corresponding product yields (H atoms and CH_3) increases. The reduction of the species CH_3 on the surface forces low-temperature H atoms to form H_2 rather than CH_4. On the other hand, high-temperature H atoms react with CH_3 to form CH_4. Consequently, the production of high-temperature CH_4 increases at the expense of the low-temperature CH_4 production, which is in agreement with available experiments.[38]

Products from HCHO. The produced HCHO from the C−H bond scission of CH_3O may desorb from the surface by absorbing the heat of 2.52 eV. It can also undergo successive dehydrogenation to yield CO ($HCHO \xrightarrow{-H} CHO \xrightarrow{-H} CO$) or via the path $HCHO \xrightarrow{-O} CH_2 \rightarrow C_2H_4$ to yield C_2H_4. Detailed descriptions for these two paths have been reported in our previous work.[58] The results show that the decomposition of HCHO is kinetically and thermodynamically favored over its desorption, so in experiment only small amount of HCHO desorption was observed.[38] As discussed above, although CH_2OH is unlikely to be formed from C−H bond scission of CH_3OH at low temperature, another possible formation path of CH_2OH involving the hydrogenation of HCHO was studied. This path starts from the coadsorption state of HCHO and H and then passes through TS6 to yield CH_2OH with the $\eta^1(C)-\eta^1(O)$ configuration as shown in Figure 6. The energy barrier of this path is much larger, 2.00 eV, and the reaction energy is 1.89 eV, suggesting that CH_2OH is unlikely to be formed on V(100) at low temperature and its following decomposition can be neglected in the reaction network. Considering the possibility of HCHO oxidation on O-prodosed V(100), the reactions $CH_xO + O \rightarrow CH_xO_2$ ($x = 0-2$) were studied. The results show that those reactions are very

dx.doi.org/10.1021/jp307760a | J. Phys. Chem. C 2012, 116, 25344−25353

Table 2. Calculated Activation Barriers E_{act} (eV) after ZPE Corrections and Reaction Rates (in s^{-1}) for Elementary Steps under Typical UHV Conditions (100 K< T < 550 K, $p = 2 \times 10^{-10}$ Torr)

surface reactions		rates						
		100 K	200 K	260 K	320 K	400 K	500 K	550 K
1. $CH_3OH(g) + * \leftrightarrow CH_3OH*$								
2. $CH_3OH* + * \rightarrow CH_3O* + H*$	0.05	1.58×10^{-98}	4.88×10^{-44}	2.00×10^{-31}	1.59×10^{-23}	1.17×10^{-16}	3.76×10^{-11}	2.78×10^{-9}
3. $CH_3O* + * \rightarrow CH_3* + O*$	0.79	1.58×10^{-98}	4.88×10^{-44}	2.00×10^{-31}	1.59×10^{-23}	1.17×10^{-16}	3.75×10^{-11}	2.78×10^{-9}
4. $CH_3O* + * \rightarrow HCHO* + H*$	1.11	1.26×10^{-114}	4.35×10^{-52}	1.28×10^{-37}	1.48×10^{-28}	1.11×10^{-20}	2.26×10^{-14}	3.29×10^{-12}
5. $CH_3* + H* \rightarrow CH_4(g) + 2*$	1.03[a]	1.58×10^{-98}	4.88×10^{-44}	2.00×10^{-31}	1.59×10^{-23}	1.17×10^{-16}	3.75×10^{-11}	2.78×10^{-9}
6. $HCHO* + * \rightarrow CHO* + H*$	0.38[a]	1.26×10^{-114}	4.35×10^{-52}	1.28×10^{-37}	1.48×10^{-28}	1.11×10^{-20}	2.25×10^{-14}	3.26×10^{-12}
7. $CHO* + * \rightarrow CO* + H*$	0.27[a]	1.26×10^{-114}	4.35×10^{-52}	1.28×10^{-37}	1.48×10^{-28}	1.11×10^{-20}	2.25×10^{-14}	3.26×10^{-12}
8. $H* + H* \rightarrow H_2(g) + 2*$	1.37	1.26×10^{-114}	8.70×10^{-52}	2.57×10^{-37}	2.97×10^{-28}	2.21×10^{-20}	4.51×10^{-14}	6.55×10^{-12}
9. $HCHO* + * \rightarrow CH_2* + O*$	0.61[a]	3.36×10^{-126}	7.12×10^{-58}	4.55×10^{-42}	3.59×10^{-32}	1.42×10^{-23}	1.09×10^{-16}	2.57×10^{-14}
10. $CH_2* + CH_2* \rightarrow C_2H_4* + *$	2.71[a]	1.68×10^{-126}	3.56×10^{-58}	2.27×10^{-42}	1.79×10^{-32}	7.08×10^{-24}	5.45×10^{-17}	1.28×10^{-14}
11. $CO* \rightarrow CO(g) + *$	E_{ad}^{CO}	1.26×10^{-114}	4.35×10^{-52}	1.28×10^{-37}	1.48×10^{-28}	1.11×10^{-20}	2.25×10^{-14}	3.26×10^{-12}
12. $C_2H_4* \rightarrow C_2H_4(g) + *$	0.57	1.68×10^{-126}	3.56×10^{-58}	2.27×10^{-42}	1.79×10^{-32}	7.08×10^{-24}	5.45×10^{-17}	1.28×10^{-14}

[a]Values are taken from our previous work, ref 58.

endothermic and have large barriers, which means the final product CO_2 cannot be formed at normal temperature, same as the experimental observation.[38]

Formation of H_2O. Considering that small amount of H_2O was observed on V(100), we studied the possible formation path of OH from the reaction of O and H atoms, which are easily formed on the surface as discussed above. In this path (see Figure 6), the H atom at one hollow site and the O atom at the adjacent hollow site pass through a transition state to yield OH at the same hollow site as O. And then OH diffuses to its favorite bridge site with an adsorption energy of −4.66 eV. This step has to overcome a barrier of 2.27 eV and is endothermic by 2.18 eV. So the formation of OH from O and H atoms is very difficult, which means that H_2O cannot be formed from the path $O + H \rightarrow OH \xrightarrow{+H} H_2O$ on clean V(100).

On the other hand, there is less possibility for OH formation from the C−O bond scission of CH_3OH (with a barrier of 0.65 eV) or the H-abstraction reactions on O-predosed surface (such as $CH_3OH + O \rightarrow CH_3O + OH$, with a barrier of 0.69 eV); thus, two paths for the formation of H_2O from OH were studied and are shown in Figure 6. One path is OH at bridge site reacts with H at adjacent hollow site to yield H_2O. This reaction requires overcoming a large barrier of 1.75 eV at TS8 and is endothermic by 1.78 eV relative to the coadsorption initial state with an attractive interaction of 0.03 eV. The nascent H_2O adsorbs at its most favorable top site through O with the O−H bonds both parallel to the surface and the adsorption energy is −0.60 eV. An alternative path is offered by OH disproportionation. Both OH coadsorb at bridge sites with an attractive interaction energy of 0.17 eV, and the formed H_2O and O show a repulsive interaction energy of 0.06 eV. This is a very facile step, with a smaller barrier of 0.53 eV and is modestly endothermic by 0.07 eV relative to the reactants at coadsorption state. Thus, H_2O can be formed from the disproportionation of OH produced on the surface rather than from the combination of H and OH (or O), which is in line with the experimental speculation.[38]

3.5. Microkinetic Model. In order to give a further interpretation of the selectivity trends of the decomposition pathways of methanol, a 12-step microkinetic model was developed on the basis of our DFT results and shown in Table 2. Typical pre-exponential factors[59] of 10^{13} s^{-1} combined with the calculated energy barriers on the clean surface were used to calculate the actual reaction rate constants of the elementary steps. The adsorption and desorption of methanol were assumed to be in equilibrium. For other steps, the pseudo-steady-state approximation was applied. The reverse reactions of the elementary steps were not included in the model because the decomposition process is nearly irreversible and the products desorb quite readily under UHV condition. On the basis of the fact that only the adsorption energies of CH_3OH, CO, and C_2H_4 were the parameters of the microkinetic model and the coverages of CH_3OH and C_2H_4 were estimated to be very low under all the considered conditions by the microkinetic model, only the coverage effect of CO was incorporated into the model. Additional calculations for the adsorption energy of CO on V(100) as a function of coverage (θ_{CO}) yield the following relation: $E_{ad}^{CO} = 2.93\theta_{CO}^2 - 2.40\theta_{CO} - 2.85$ eV. Overall, we solved eight steady-state equations for the fractional surface coverage of the adsorbed species together with one site-balance equation. The detailed description of the microkinetic model is given in the Supporting Information. The estimated rate of each steps under the UHV condition (100 K< T < 550 K, $p = 2 \times 10^{-10}$ Torr) corresponding to a very low O* coverage ($\theta_O = 0$) are given in Table 2, and the rates for yielding CH_4, CO, and C_2H_4 as a function of temperature are plotted in Figure 7. The effect of O coverage on the decomposition process will be discussed in a later paragraph.

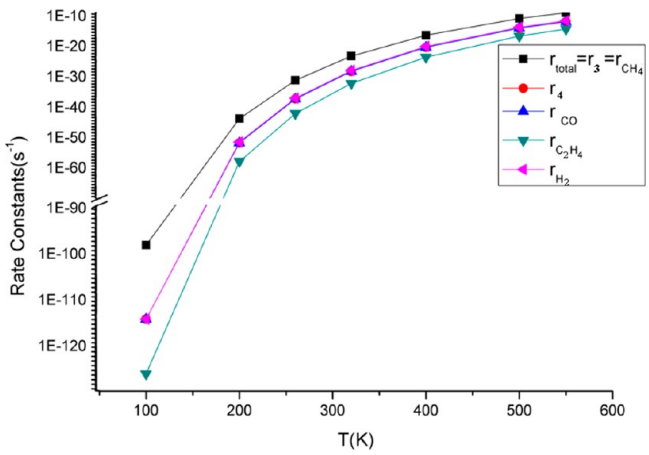

Figure 7. Temperature dependence of the rates for methanol decomposition, methoxy decomposition, and products formations on V(100) using the microkinetic modeling technique.

dx.doi.org/10.1021/jp307760a | J. Phys. Chem. C 2012, 116, 25344−25353

A comparison of the rates of various elementary steps included in the model reveals that rates of steps for CH_4 formation (steps 3 and 5 in Table 2) are almost the same as the rate of the O−H bond scission of CH_3OH under the investigated conditions, and rates of steps (6−10) beginning with C−H bond scission of CH_3O contribute less to the decomposition pathway, although the latter steps become slightly more important as the temperature increases. These results clearly suggest that the methanol decomposition on clean V(100) involves predominantly the path $CH_3OH \rightarrow CH_3O \rightarrow CH_3 \rightarrow CH_4$, while the other path involving $CH_3O \rightarrow HCHO$ to produce CO or/and C_2H_4 does not play a significant role in the overall ration network. So CH_4 is the major product for the decomposition of CH_3OH, while CO and C_2H_4 formations cannot compete with it as shown in Figure 7. This is consistent with the experimental observation.[38]

To identify the effect of surface O on the product selectivity, we performed a microkinetic analysis by artificially and independently changing some variables in the kinetic model. The first changed value is only O* coverage on the surface. It is found that the rate for each step becomes smaller as the increasing of O* coverage, while the product selectivity remains almost the same. In addition, we changed the adsorption energy of CH_3OH to that corresponding to the coverages of 0.25 and 0.11 ML while keeping other variables constant. It is found that the rates for all steps in this model stay the same. Furthermore, we replaced the decomposition barriers of CH_3O by our calculated DFT values on O-predosed surface at the coverages of 0.11 and 0.25 ML. It is shown that the rates for R2 ($CH_3OH^* + * \rightarrow CH_3O^* + H^*$), R3 ($CH_3O^* + * \rightarrow CH_3^* + O^*$), and R5 ($CH_3^* + H^* \rightarrow CH_4(g) + 2^*$) decrease while the values for other steps do not change. Finally, we calculated the rates under the condition of O coverages of 0.11 and 0.25 ML on the surface, respectively, combined with the energy barriers on the O-predosed surface. It is found that all rates are reduced while the ratio of the rates for the C−H bond scission of CH_3O relative to the C−O bond scission is increased, which leads to the enhanced ratio of the high-temperature CH_4 yield to the low-temperature CH_4 yield. In addition, it is seen that the rates at the coverage of 0.25 ML are lower than those at 0.11 ML, while the ratio of the rates for the above two steps is larger, indicating that the effect of the O coverage increases in the range below 0.25 ML. These results are consistent with the experimental observation that the presence of oxygen on the surface below 0.3 ML enhances the yield of the high-temperature methane state at expense of the low-temperature methane production and delays all surface reactions to higher temperature.[38]

4. CONCLUSION

Using periodic DFT calculation, we obtained the potential energy diagrams and developed a simple microkinetic model to describe the possible paths of methanol decomposition on clean and O-predosed V(100) surfaces. Our results show that the O−H bond scission of CH_3OH is the most favorable path both in kinetics and thermodynamics, while the C−H and C−O bond scissions are unlikely to occur on V(100) at low temperature due to the higher energy barriers compared with the weak interaction between CH_3OH and the surface. CH_3O is the major intermediate, which can be formed even at the very low temperature; at the same time part of the produced H atoms combine to form H_2 leaving from the surface driven by the entropic effect. As temperature increases, the decomposition of CH_3O occurs via the C−O dissociation to form CH_3 at around 316 K, which is followed by reacting with the H atoms that remained on the surface to yield CH_4 at low temperature. The C−H bond scission of CH_3O to form HCHO is slightly difficult than the C−O bond scission and can occur at higher temperature around 444 K, and then HCHO will undergo decomposition or/and coupling to form CO or/and C_2H_4. The H atoms produced from the dehydrogenation process of CH_3O are responsible for the formation of CH_4 at the high temperature region. The inhibition effect of the coadsorbed oxygen on the C−O and C−H bond scissions of CH_3O in different degrees leads to the increasing of the yield ratio of CH_4 at high-temperature region to that at low-temperature region. Likewise, the other products from the dissociation of CH_3O are all delayed to higher temperature. Our calculated results are in agreement with the experimental observations and speculation.[38]

■ ASSOCIATED CONTENT

Supporting Information

Detailed information on microkinetic modeling. This material is available free of charge via the Internet at http://pubs.acs.org.

■ AUTHOR INFORMATION

Corresponding Author

*E-mail: ljy121@jlu.edu.cn.

Notes

The authors declare no competing financial interest.

■ ACKNOWLEDGMENTS

This work was supported by the National Nature Science Foundation of China (20973077, 20303007), US National Science Foundation (Award 1012994), and the Program for New Century Excellent Talents in University (NCET).

■ REFERENCES

(1) Kartha, S.; Grimes, P. *Phys. Today* **1994**, *47*, 54−61.
(2) Strasser, P.; Fan, Q.; Devenney, M.; Weinberg, W. H.; Liu, P.; Nørskov, J. K. *J. Phys. Chem. B* **2003**, *107*, 11013−11021.
(3) Balm, P. K.; Kim, H. S.; Oldfield, E.; Wieckowski, A. *J. Phys.Chem. B* **2003**, *107*, 7595−7600.
(4) Huber, G. W.; Shabaker, J. W.; Dumesic, J. A. *Science* **2003**, *300*, 2075−2078.
(5) Gupta, S.; Datta, J. J. *Chem. Sci.* **2005**, *117*, 337−344.
(6) Gojković, S. L. J.; Tripković, A. V.; Stevanović, R. M. *J. Serb. Chem. Soc.* **2007**, *72*, 1419−1425.
(7) Liu, H. P.; Ye, J. Q.; Xu, C. W.; Jiang, S. P.; Tong, Y. X. *J. Power Sources* **2008**, *177*, 67−70.
(8) Queeney, K. T.; Friend, C. M. *J. Chem. Phys.* **1998**, *109*, 6067−6074.
(9) Chen, Z. X.; Neyman, K. M.; Lim, K. H.; Rösch, N. *Langmuir* **2004**, *20*, 8068−8077.
(10) Krenn, G.; Schennach, R. *J. Chem. Phys.* **2004**, *120*, 5729.
(11) Sim, W. S.; Gardner, P.; King, D. A. *J. Phys. Chem.* **1995**, *99*, 16002−16010.
(12) Bae, S.-S.; Kim, D. H.; Kim, A.; Jung, S. J.; Hong, S.; Kim, S. *J. Phys. Chem. C* **2007**, *111*, 15013−15019.
(13) Boccuzzi, F.; Chiorino, A.; Manzoli, M. *J. Power Sources* **2003**, *118*, 304−310.
(14) Henry, H. H.; Chen, J. G. G. *J. Phys. Chem. B* **2003**, *107*, 2029−2039.
(15) Barros, R. B.; Garcia, A. R.; Ilharco, L. M. *J. Phys. Chem. B* **2004**, *108*, 4831−4839.
(16) Habermehl-Cwirzen, K.; Lahtinen, J.; Hautojärvi, P. *Surf. Sci.* **2005**, *598*, 128−135.

(17) Vinod, C. P.; Niemantsverdriet, J. W.; Nieuwenhuys, B. E. *Phys. Chem. Chem. Phys.* **2005**, *7*, 1824−1829.
(18) Kubota, J.; Kusafuka, K.; Wada, A.; Domen, K.; Kano, S. S. *J. Phys. Chem. B* **2006**, *110*, 10785−10791.
(19) Weststrate, C. J.; Ludwig, W.; Bakker, J. W.; Gluhoi., A. C. *J. Phys. Chem. C* **2007**, *111*, 7741−7747.
(20) Wang, G.-C.; Zhou, Y.-H.; Morikawa, Y.; Nakamura, J.; Cai, Z.-S.; Zhao, X.-Z. *J. Phys. Chem. B* **2005**, *109*, 12431−12442.
(21) Xu, L.; Mei, D.; Henkelman, G. *J. Chem. Phys.* **2009**, *131*, 244520.
(22) Sakong, S.; Groß, A. *J. Catal.* **2005**, *231*, 420−429.
(23) Sakong, S.; Gross, A. *J. Phys. Chem. A* **2007**, *111*, 8814−8822.
(24) Mei, D.; Xu, L.; Henkelman, G. *J. Phys. Chem. C* **2009**, *113*, 4522−4537.
(25) Gu, X.-K.; Li, W.-X. *J. Phys. Chem. C* **2010**, *114*, 21539−21547.
(26) Greeley, J.; Mavrikakis, M. *J. Am. Chem. Soc.* **2004**, *126*, 3910−43919.
(27) Kandoi, S.; Greeley, J.; Sanchez-Castillo, M. A.; Evans, S. T.; Gokhale, A. A.; Dumesic, J. A.; Mavrikakis, M. *Top. Catal.* **2006**, *37*, 17−28.
(28) Desai, S. K.; Neurock, M.; Kourtakis, K. *J. Phys. Chem. B* **2002**, *106*, 2559−2568.
(29) Jiang, R.; Guo, W.; Li, M.; Fu, D.; Shan, H. *J. Phys. Chem. C* **2009**, *113*, 4188−4197.
(30) Jiang, R.; Guo, W.; Li, M.; Zhu, H.; Zhao, L.; Lu, X.; Shan, H. *J. Mol. Catal. A: Chem.* **2011**, *344*, 99−110.
(31) Montoya., A.; Haynes, B. S. *J. Phys. Chem. C* **2007**, *111*, 9867−9876.
(32) Chen, W.-.K.; Liu, S.-H.; Cao, M.-J.; Yan, Q.-G.; Lu, C.-H. *J. Mol. Struct.: THEOCHEM* **2006**, *770*, 87−91.
(33) Spencer, N. D.; Pereira, C. J. *J. Catal.* **1989**, *116*, 399−406.
(34) Arena, F.; Parmaliana, A. *Acc. Chem. Res.* **2003**, *36*, 867−875.
(35) Weckhuysen, B. M.; Keller, D. E. *Catal. Today* **2003**, *78*, 25−46.
(36) Wong, G. S.; Concepcion, M. R.; Vohs, J. M. *J. Phys. Chem. B* **2002**, *106*, 6451−6455.
(37) Magg, N.; Giorgi, J. B.; Schroeder, T.; Bäumer, M.; Freund, H.-J. *J. Phys. Chem. B* **2002**, *106*, 8756−8761.
(38) Shen, M.; Zaera, F. *J. Phys. Chem. C* **2008**, *112*, 1636−1644.
(39) Sim, W. S.; Gardner, P.; King, D. A. *Surf. Rev. Lett.* **1994**, *1*, 673−686.
(40) Wachs, I. E.; Madix, R. J. *Surf. Sci.* **1978**, *76*, 531−558.
(41) Wang, J.; Xu, X.; Deng, J.; Liao, Y.; Hong, B. *Appl. Surf. Sci.* **1997**, *120*, 99−105.
(42) Gates, J. A.; Kesmodel, L. L. *J. Catal.* **1983**, *83*, 437−445.
(43) Gong, J.; Flaherty, D. W.; Ojifinni, R. A.; White, J. M.; Mullins, C. B. *J. Phys. Chem. C* **2008**, *112*, 5501−5509.
(44) Davies, P. R.; Mariotti, G. G. *J. Phys. Chem.* **1996**, *100*, 19975−19980.
(45) Shu-Xia, T.; Gui-Chang, W.; Xian-He, B. *J. Phys. Chem. B* **2006**, *110*, 26045−26054.
(46) Perdew, J. P.; Burke, K.; Ernzerhof, M. *Phys. Rev. Lett.* **1996**, *77*, 3865−3868.
(47) Kresse, G.; Hafner, J. *Phys. Rev. B* **1993**, *47*, 558−561.
(48) Kresse, G.; Furthermüller, J. *Phys. Rev. B* **1996**, *54*, 11169−11186.
(49) Blöchl, P. E. *Phys. Rev. B* **1994**, *50*, 17953−17979.
(50) Kresse, G.; Joubert, D. *Phys. Rev. B* **1999**, *59*, 1758−1775.
(51) Wyckoff, R. W. G. *Crystal Structures*; Interscience Publishers: New York, 1963.
(52) Henkelman, G.; Uberuaga, B. P.; Jónsson, H. *J. Chem. Phys.* **2000**, *113*, 9901−9904.
(53) Henkelman, G.; Jónsson, H. *J. Chem. Phys.* **2000**, *113*, 9978−9985.
(54) McKay, H. L.; Jenkins, S. J.; Wales, D. *J. Phys. Chem. C* **2009**, *113*, 15274−15287.
(55) Tang, W.; Sanville, E.; Henkelman, G. *J. Phys.: Condens. Matter* **2009**, *21*, 084204.
(56) Sanville, E.; Kenny, S. D.; Smith, R.; Henkelman, G. *J. Comput. Chem.* **2007**, *28*, 899−908.
(57) Henkelman, G.; Arnaldsson, A.; Jónsson, H. *Comput. Mater. Sci.* **2006**, *36*, 254−360.
(58) Wang, H.; He, C.-Z.; Huai, L.-Y.; Liu, J.-Y. *J. Phys. Chem. C* **2012**, *116*, 10639−10648.
(59) Dumesic, J. A.; Rudd, D. F.; Aparicio, L. M.; Rekoske, J. E.;Treviño, A. A. *The Microkinetics of Heterogeneous Catalysis*; American Chemical Society: Washington, DC, 1993; p 40.